Accepted Manuscript

Decoupling the autogenous swelling from the self-desiccation deformation in early age concrete with mineral additions: Micro-macro observations and unified modelling

Jérôme Carette, Shiju Joseph, Özlem Cizer, Stéphanie Staquet

PII: S0958-9465(16)30737-5

DOI: 10.1016/j.cemconcomp.2017.10.008

Reference: CECO 2924

To appear in: *Cement and Concrete Composites*

Received Date: 17 November 2016

Revised Date: 23 August 2017

Accepted Date: 19 October 2017

Please cite this article as: Jéô. Carette, S. Joseph, Ö. Cizer, Sté. Staquet, Decoupling the autogenous swelling from the self-desiccation deformation in early age concrete with mineral additions: Micro-macro observations and unified modelling, *Cement and Concrete Composites* (2017), doi: 10.1016/j.cemconcomp.2017.10.008.

Decoupling the autogenous swelling from the self-desiccation deformation in early age concrete with mineral additions: micro-macro observations and unified modelling

Jérôme Carette[1], Shiju Joseph[2], Özlem Cizer[2], Stéphanie Staquet[1]

[1] BATir department, Université Libre de Bruxelles (ULB), Brussels, Belgium

[2] Department of Civil Engineering, Katholieke Universiteit Leuven (KUL), Leuven, Belgium

1. Introduction

Supplementary cementitious materials (SCM) are commonly used as cement substitution in concrete materials for technical, economical or environmental benefits. In order to reduce the carbon footprint of concrete coming from the important CO_2 emissions related to clinker production, the massive replacement of Portland cement by a combination of limestone filler (LMF) and blast furnace slag (BFS) has already been proven to be effective from a mechanical behaviour perspective. The impact of such concrete mixes on the concrete setting, strength, elastic modulus or heat release has been at the centre of the attention for the last decade [01, 02, 03, 04, 05, 06, 07]. These studies have highlighted the mechanisms at the origin of the effect of LMF and BFS on these properties, and have resulted in the adaptation of the existing models in order to take into account their respective effects.

However, there exist few comprehensive studies assessing the effect of these combined SCM on the early age deformation potential of concrete [08, 09]. In particular, the prediction of the autogenous deformation of such mixes remains of major interest as there lacks simple models that can be applied to SCM-based concrete. This lack of model can be explained by the recent interest brought by the scientific community to the behaviour of concrete at early age, and also to the complex issue of the autogenous deformation, which is the combination of various combined mechanisms. Indeed, these mechanisms include chemo-mechanical consequences of hydration, such as self-desiccation or chemical swelling, as well as volumetric changes induced by temperature variations.

In 2005, Barcelo et al first formally suggested that the autogenous deformation in isothermal conditions results from the coupling of a swelling deformation, related to the formation of hydration products and the self-desiccation deformation resulting from water-related processes [10]. The mechanisms at the origin of this swelling have been widely studied in the past decades. They include measurement artefacts, absorption of bleeding water [11], water adsorption by fillers [12, 13], CH growth [14] and primary ettringite formation [14, 15]. Even if there is still no general agreement as to which of the aforementioned mechanisms is the dominating one, it remains clear that both LMF and BFS generate early age swellings deformations.

There exist plenty of models describing the evolution of the autogenous deformation with empirical models expressed as a function of time, degree of hydration or relative humidity [16, 17, 18, 19] as well as more complex microstructural approaches [20]. However, none of these models consider the early age swelling behaviour, as they were mostly developed for hardening Portland cement concrete. Therefore, these models are either unadapted to the very early age behaviour, or unable to express the sensitivity of the autogenous deformation to the type of

SCM. In order to be able to include all these processes in one unified model, the first step consists in decoupling the self-desiccation deformation from the swelling deformation.

The aim of this paper is to

- present a new methodology in order to decouple the early age swelling deformation from the self-desiccation deformation,
- apply this methodology to various concrete composition containing various amounts and nature of SCM,
- link the swelling deformation to the microstructure development,
- unify the observed processes in a single hydration-based model.

2. Materials and method

2.1.Materials

The materials used for this study are a CEM I 52.5 N, limestone micro-filler, blast-furnace slag and gypsum. Their chemical compositions are detailed in Table 1.

Table 1. Composition and physical properties of materials

		CEM I	BFS	LMF	Gypsum
C_2S	[%]	12.6	-	-	-
C_3S	[%]	63.49	-	-	-
C_3A	[%]	8.09	-	-	-
C_4AF	[%]	9.8	-	-	-
SiO_2	[%]	20.12	33.3	-	-
Al_2O_3	[%]	5.03	12.5	-	-
CaO	[%]	64.53	41.5	-	-
MgO	[%]	0.98	7	-	-
$CaCO_3$	[%]	-	-	98	-
$CaSO_4$	[%]	4.5	-	-	79
SO_3	[%]	3.36	0.16	0.00	46.5
blaine	[cm^2/g]	365	450	647	354
density	[kg/m^3]	3.15	2.89	2.71	2.31

Four concrete compositions are studied (Table 2). Two compositions containing high amounts of limestone filler (C3) and blast furnace slag (C2) are investigated, as well as a reference mix with a binder containing only Portland cement (C1). Then, a fourth concrete is tested for the combined effect of both additions (C4). The binders therefore include variable contents of cement, LMF, BFS and gypsum. Amongst all these compositions, it is ensured that the granular skeleton, water/binder ratio (w/b), paste volume and sulphate content are constant. The constant sulphate content was ensured by modifying the amount of gypsum between compositions. The binder content includes the cement, gypsum, BFS and LMF. The properties of these concrete mixes shown in the following table are extracted from [06, 07]. If limestone filler is considered as inert, a water/reactive ration (w/r) can be computed, by considering only cement, slag and gypsum in the reactive binder content. The apparent activation energy E_a describes the sensitivity of the hydration reactions to temperature variations. The final setting time is noted t_0.

Table 2. Composition and properties of concrete mixtures (kg/m3)

	C1	C2	C3	C4
Aggregate 10/14	873	873	873	873
Aggregate 6/10	210	210	210	210
Sand 0/4	853	853	853	853
CEM I 52.5	432	104	285	103
BFS	0	291	0	164
LMF	0	0	126	124
Gypsum	0	22	10	22
Water	173	167	169	165
Density [kg/m³]	2540	2519	2525	2514
w/b	0.4	0.4	0.4	0.4
w/r	0.4	0.4	0.57	0.57
E_a [kJ/mol]	35.9	51.1	39.1	49.7
t_0 [h]	4.1	8.5	4.6	6.8
E_s 28d [GPa]	51.8	51.7	48.4	50.0
f_c 28d [MPa]	53.2	38.7	46.4	33.8
f_c 90d [MPa]	58.3	44.0	48.6	39.6
f_c 365d [MPa]	61.4	49.6	52.3	46.3
slump class	S1	S1	S3	S2

2.2. *Test setup*

2.2.1. *Setting time*

As soon as the concrete is cast in its moult, deformations occur, such as plastic shrinkage, chemical shrinkage and thermal deformations. However, before the setting of concrete, these deformations have no impact on the structural behaviour of concrete, as they do not induce internal stresses in the material. In this study, the autogenous deformation is defined as any deformation occurring without external mechanical loading, water exchange with the environment, or heating of the material, which could induce internal stresses inside the material. Therefore, these deformations are not measured before final setting (t_0). The final setting time is determined by the dynamic elastic modulus as computed from continuous ultrasonic monitoring of P-wave and S-wave during the first hours after casting [05]. The final setting time corresponds to the inflection point of the dynamic elastic modulus versus time curve. This criteria was suggested by comparison of the ultrasonic method with ASTM C403 standard, and measurement of very early age stiffness and strength gain. This methodology as well as the corresponding test setup and results for the tested materials are presented elsewhere [05]. The values of t_0 for each composition are shown in Table 2.

2.2.2. *Degree of hydration*

The decoupling strategy presented in this paper requires the knowledge of the degree of hydration for each composition. The degree of hydration is determined from heat flow measurement with an 8-channel TAM Air isothermal calorimeter. These measurements are performed on mortars corresponding to mixes C1, C2, C3 and C4, without large aggregates, and were already presented in a previous publication [06]. Two samples of each mix are measured. The degree of hydration is obtained based on the model developed by Freisleben-Hansen and Pedersen [16], which was adapted (equations 1-3) to the hydration of SCM-based materials [06]. This model superimposes two s-shaped curves, with respective amplitudes a_1 and a_2 [J/g], time constants τ_1 an τ_2 [h], and exponents β_1 and β_2 [-]. The ultimate heat release Q_∞ [J/g] can be approximated by the sum of the amplitude parameters, and the degree of hydration $\alpha(t)$ is obtained by dividing the cumulated heat release by Q_∞.

$$Q(t) = a_1 . e^{-\left(\frac{\tau_1}{t}\right)^{\beta_1}} + a_2 . e^{-\left(\frac{\tau_2}{t}\right)^{\beta_2}} \quad (1)$$

$$Q_\infty = a_1 + a_2 \quad (2)$$

$$\alpha(t) = \frac{Q(t)}{Q_\infty} \quad (3)$$

2.2.3. *TGA analysis*

The amount of portlandite and the qualitative estimation of ettringite content are determined through thermogravimetric analysis (TGA). Hydration was stopped using a freeze dryer (2 hours at 0.03 mbar) after gently crushing the samples. The mass loss of cement samples submitted to temperatures between 25 and 900 °C is measured. The samples mass was between 25mg and 35mg. The instrument used for this purpose was a NETZSCH STA 409 PC, operated in nitrogen atmosphere, at a controlled heating rate of 10 °C/min and flow rate 60 mL/min. The first derivative of thermogravimetry (DTG) was used to identify the reaction products.

2.2.4. *Autogenous deformations*

Due to the necessity of carrying out tests on concrete samples since the setting time in isothermal conditions, a specific testing device called BTJADE was used [21]. Specifically designed for such purposes, it allows the vertical measurement of the displacements of a concrete specimen placed in a thermally regulated liquid bath (Figure 1). It mainly consists of a test rig, composed of a PVC corrugated mould and fixed metallic parts. The whole system is placed into an isolated thermo-controlled bath to ensure the autogenous conditions, namely a temperature as constant as possible, a stress free state and a protection against desiccation. On the sample, different sensors (displacement, temperature) are installed.

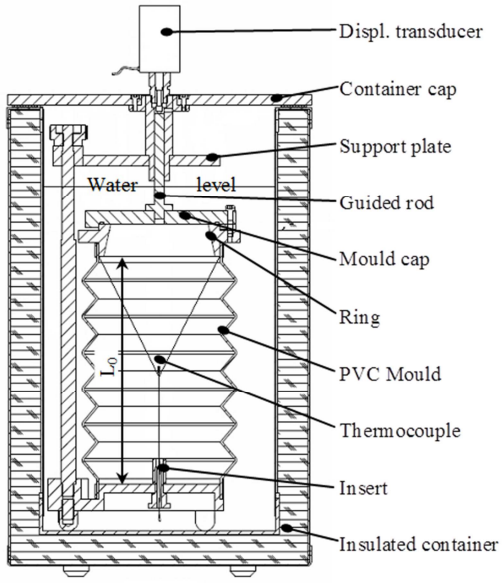

Figure 1. BTJADE test setup

This setup allows a very precise measurement of the length variation Δl_m of a concrete sample in order to compute the total autogenous deformations ε_{au}. Calibrated coefficients (C_w and C_a) taking into account the response of the test setup to a temperature variation of the ambient air θ_a or water in the tank θ_w permit to subtract these measurement artefact to the actual concrete deformations (equation 4). The flexibility of the PVC mould allows measuring deformation from the earliest age to several months. Up to three samples of length L_0 can be simultaneously monitored in the same water bath.

$$\varepsilon_{au} = \frac{\Delta l_m - C_w \Delta\theta_w - C_a \Delta\theta_a}{L_0} \quad (4)$$

For each concrete composition, at least three samples were tested, resulting from at least two batches of the same composition. The data treatment allows taking into account the thermal strains by measuring the temperature of the sample θ_c at all times, provided that the concrete coefficient of thermal expansion C_{te} is known. This setup allows a direct measurement of C_{te} by measuring the sample displacements for a given bath temperature variation. The measurement of the autogenous deformation is measured from casting up to several weeks.

2.3.*Decoupling approach*

Various processes occur at early age, resulting in the overall measured autogenous deformation. They appear in Figure 2, which is a more complete vision of the scheme suggested by Barcelo et al [10]. The three processes shown are only considered after the final setting. The self-desiccation deformation ε_{sd} is caused by capillary pressure development in the porosity of the concrete. This capillary pressure occurs due to the fact that water is consumed by hydration, and that its volume is not fully replaced by hydrates. The thermal deformation ε_{th} cannot be avoided due to hydration reactions, and must be removed from the measured deformation in order to yield the autogenous deformation. The early age swelling deformation ε_{sw} can appear for various reasons:

- it is affected by measurement artefacts, which can originate from incorrect temperature-related corrections to the measurement, or from the difference between linear versus vertical measurements, as well as linear versus volumetric measurements of the deformation.
- water absorption of bleeding water by concrete leads to a swelling behaviour due to the cancelling of self-desiccation deformation [11]. Although an increase of the swelling with increasing water content is generally accepted [22], there are doubts on the fact that the cancelling of self-desiccation is its origin. In particular, there is no reason why the self-desiccation cancellation would induce swelling rather than no shrinkage at all.
- in the presence of fine particles in concrete, significant early age swelling peaks can be observed [12]. This can be observed for several filler fineness and nature, as a result of the adsorption of water by the filler, and the resulting disjointing pressure [13].
- early age swelling can occur due to the formation and growth of large size portlandite crystals [22]. This observation is mostly related to the size of the crystals rather than to their amount, as observed on various water/cement mixtures. This swelling is mainly attributed to CH crystals but can also be partially explained by the formation of C-S-H or AFt. On the other hand, Darquennes et al. opposes that in the presence of slag, high swellings are observed with constant portlandite content [23].

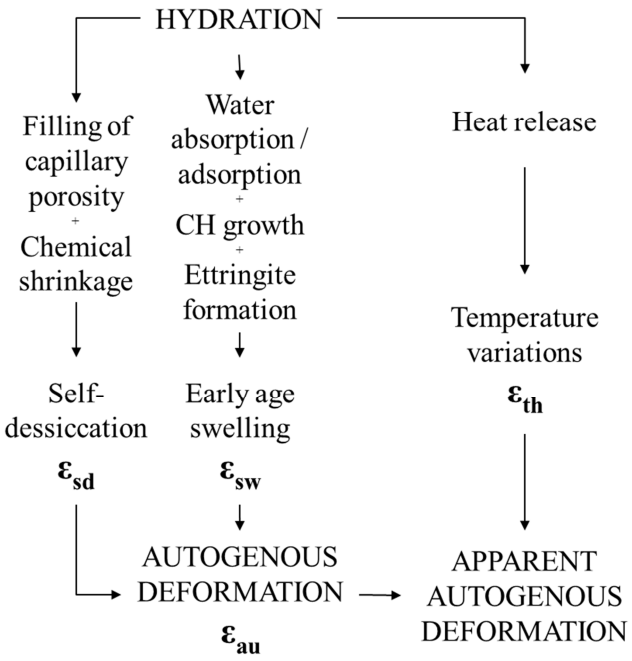

Figure 2. Causes of the autogenous deformation

The thermal deformation term in equation 5 can easily be determined by monitoring the temperature of the concrete and by measuring the coefficient of thermal expansion (C_{te}) of the concrete, as shown in equation 6. This coefficient is considered constant through hydration. The temperature in the sample is considered homogeneous.

$$\varepsilon_{measure} = \varepsilon_{au} + \varepsilon_{th} \qquad with \;\; \varepsilon_{au} = \varepsilon_{sd} + \varepsilon_{sw} \tag{5}$$

$$\varepsilon_{th} = C_{te}\Delta\theta_c \tag{6}$$

In the following section, a methodology is presented for decoupling ε_{sw} from ε_{sd} in early age concrete, as well as a strategy for the modelling of both contributions to the autogenous deformation.

3. Results and discussion

3.1. *Degree of hydration*

The degree of hydration is determined from heat release measurements, which ultimate value is determined from equation 1 and equation 2. The heat flow measurements are shown in Figure 3. The identified parameters for the model as well as the corresponding root mean square error (RSME) are shown in Table 3.

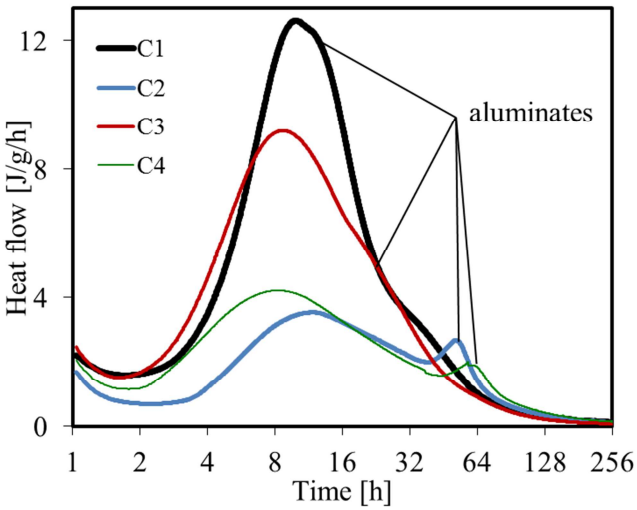

Figure 3.Heat flow measurements for all compositions

The experimental results for these compositions as well as the model parameters were already presented elsewhere [06]. The effect of LMF and BFS on the heat flow is thoroughly described in that previous study. The effect of LMF (C3) includes an acceleration of the early hydration and a decrease of the cumulated heat release. On the other hand, BFS (C2) delays the main hydration peak, decreases the cumulated heat release, and shows a second peak between two and three days after mixing. The delay in the second peak for C2 and C4 and the delay in the shoulder peak in C3 could be attributed to the additional gypsum added changing the C3A/gypsum ratio [24]. Finally, if BFS is substituted by 30% of LMF (C4), the main hydration peak is significantly accelerated, while the second peak of hydration attributed to C3A hydration is slightly delayed.

Table 3. Parameters of the hydration model

	C1	C2	C3	C4
Q_∞	406.3	265.7	336.6	274.3
a_1	290.4	222.9	264.0	221.4
a_2	104.9	31.6	25.0	48.6
τ_1	15.4	32.5	15.4	27.8
τ_2	108.0	50.1	25.5	62.5
β_1	1.2	0.8	1.0	0.7
β_2	0.4	6.3	2.5	2.7
RMSE	1.30	0.50	0.38	0.58

3.2.*Coefficient of thermal expansion*

Temperature rises in concrete samples cannot be totally avoided. Even though the BTJADE was specifically developed for isothermal tests by submerging the sample inside a thermally regulated fluid, a slight temperature variation inside the concrete is observed. Due to the efficiency of the test setup, the early age temperature increase is lower than 1°C as shown in Figure 4. These peaks of temperature are in agreement for each composition with their respective heat flow measurement. The thermal strains resulting from this temperature increase is deduced from Equation 6.

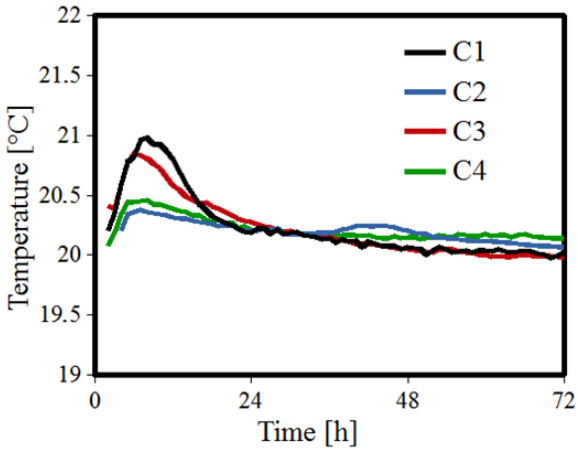

Figure 4.Temperature measurements inside the BTJADE specimens

The coefficient of thermal expansion C_{te} was measured on the four concrete compositions by measuring the displacements after having applied temperature gradients of 5°C at the end of the BTJADE tests (after 28 days). The obtained values of C_{te} are shown in Table 4. The effect of BFS content is not significant, while LMF induces a significant decrease in C_{te}. This effect can be attributed to the filler effect, which induces a lower porosity of the cement paste, as well as to the lower C_{te} of limestone itself.

Table 4. Coefficient of thermal expansion

	C1	C2	C3	C4
C_{te} [µm/m/°C]	12.4	12.5	9.7	10.7

*3.3.**Autogenous deformations***

The measurements performed on concrete samples shown in Figure 5a all exhibit a similar overall evolution. After t_0, a swelling occurs with an increasing rate. Then, a swelling peak is reached at a time between a few hours and a few days, depending on the composition. After that peak, shrinkage occurs with a decreasing rate. The shrinkage occurs as long as hydration continues. The expression of the autogenous deformation as a function of the degree of hydration is consistent with this description. Initially, the autogenous deformation shows a swelling peak that develops progressively up to a degree of hydration between 0.2 and 0.6. Then, after the peak, a shrinkage deformation progressively appears, which increases as a linear function of the degree of hydration.

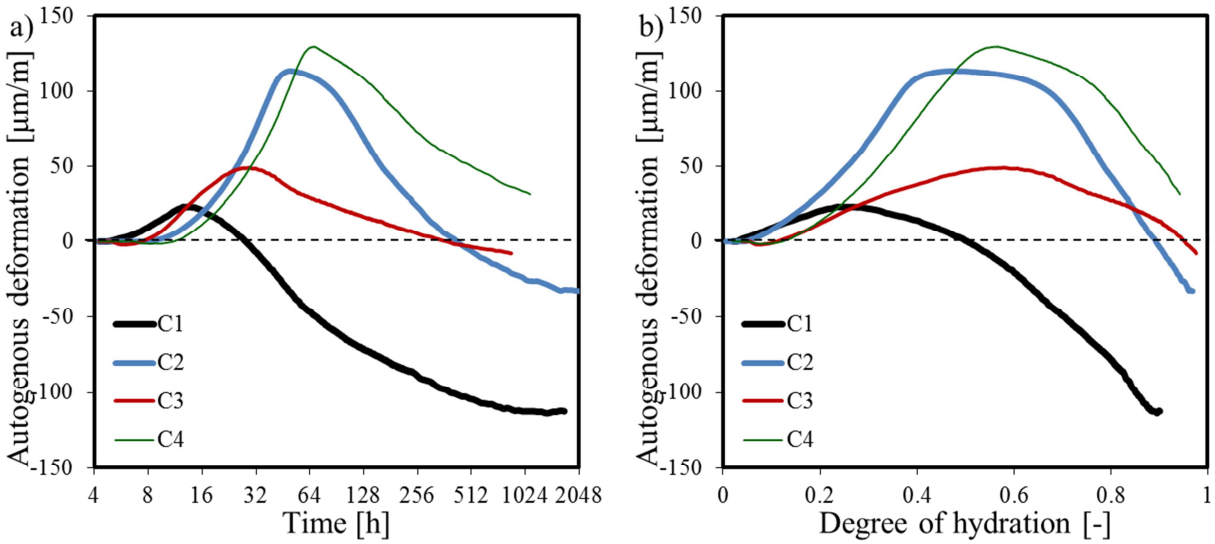

Figure 5. Autogenous deformations from BTJADE measurements as a function of (a) time and (b) degree of hydration.

The reproducibility of the measurement is shown in Figure 6a, where the continuous lines indicate the average on four samples originating from two batches of each concrete, and the dashed lines represent the maximum and minimum value for the four samples of C1 and C4. The amplitude of the swelling is not as reproducible as the slope of the shrinkage phase which is almost identical for each of the four samples. Indeed, significant variations can be observed as regards the maximal value of the autogenous deformation. This is attributed to the very early age behaviour rather than to the swelling behaviour. Indeed, since the concrete matrix has a low stiffness at very early age, the expansion might occur in the voids of the sample instead of resulting in a global increase of the sample volume. Since the samples are vibrated manually, small to moderate size air bubbles can be present in the concrete, and therefore decrease the apparent volume variations of the sample. At older ages, when the concrete is hardened enough, all expansion or shrinkage results in a measurable overall length variation, and therefore in a more reproducible measurement.

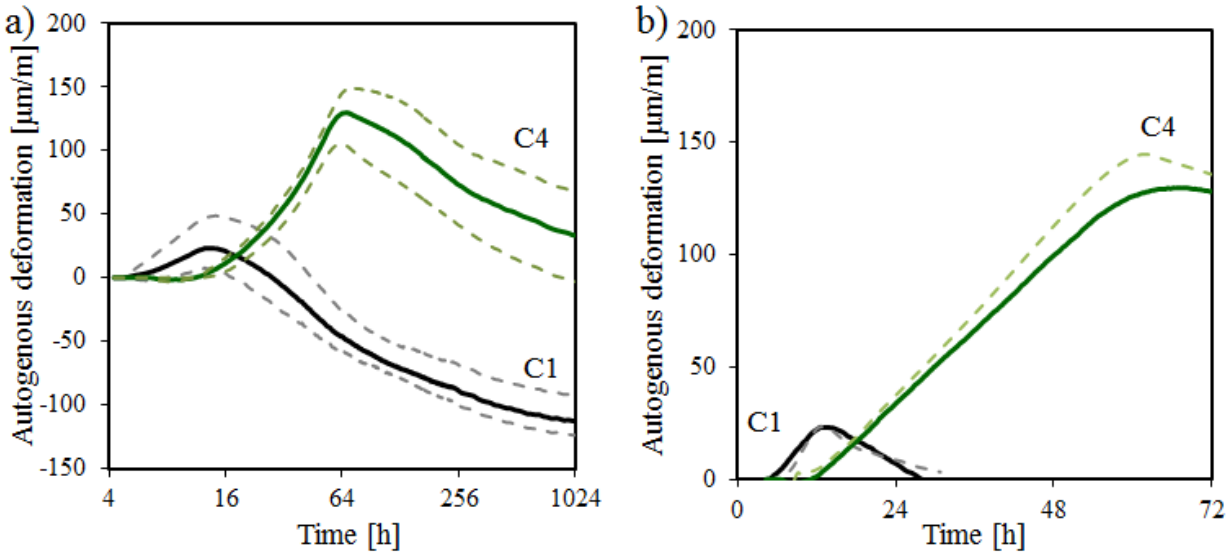

Figure 6. a) average (continuous line), maximum and minimum (dashed lines) values obtained from 4 specimens for C1 and C4 with BTJADE b) comparison between a vertical measurement (BTJADE) and horizontal measurement (TSTM) of the autogenous deformation for C1 and C4

Figure 6b shows the comparison of the measurements performed with the BTJADE device, which is a vertical measurement of the deformation with a horizontal test setup. The latter is the TSTM device, initially designed for other purpose [23], but that allows measurement of the free horizontal deformation of a 75 cm length concrete sample with a 10x10 cm section [25]. The close measurement values for both devices confirm that the observed is not a measurement artefact.

The slope of the autogenous deformation versus hydration degree (A_{sd}) is shown in Table 5. This slope is identified from after the swelling peak until several weeks. Generally, it is considered that the autogenous deformation evolves as a linear function of relative humidity (RH) inside the concrete porosity [22, 26, 16]. This makes sense since RH is representative of both the capillary pressure and the surface tension inside the material. However, it cannot be measured at very early age, when the concrete porosity is close to saturation. If no drying occurs as it is the case in this study, RH can stay close to 100% for several days [27]. In addition, shrinkage may occur when the material is still saturated, only due to the chemical shrinkage and to the overall cement matrix stiffness. Therefore, it is believed that RH is at best a partial indicator of the autogenous shrinkage at early age, and is best representative of the drying deformation of hardened concrete.

Table 5. Slope of the shrinkage deformation versus degree of hydration

	C1	C2	C3	C4
A_{sd} [µm/m]	-313±5	-446±13	-146±8	-360±12

3.3.1. *Self-desiccation deformation*

By making the assumption that the self-desiccation increases as a linear function of the degree of hydration since the setting time, it is possible to compute, for each composition, the self-desiccation deformation through equation 8. In that equation, A_{sd} is the slope shown in Table 5. In equation 7, $\tilde{\alpha}$ is defined as a function of the degree of hydration (α) and the degree of hydration corresponding to the final setting time t_0 (α_0). From a physical point of view, this assumption is not strictly accurate since the shrinkage process results from the combination of mechanisms including chemical shrinkage, decrease of capillary pressure due to water consumption and stiffness of the cement matrix. However, from a phenomenological perspective, when considering the early age behaviour (when hydration still occurs at a significant rate), all these phenomena are related to the degree of hydration. Therefore, it makes sense to relate the self-desiccation deformation to its underlying cause, i.e. the hydration process [28,29]. As a matter of fact, the autogenous self-desiccation can be modelled using similar equations as the hydration model presented in equation 1 [19].

$$\tilde{\alpha} = \frac{\alpha(t)-\alpha_0}{1-\alpha_0} \quad (7)$$

$$\varepsilon_{sd} = A_{sd} \,.\, \tilde{\alpha} \quad (8)$$

This approach is illustrated in Figure 7a. It results in strictly decreasing negative deformations (shrinkage), which ultimate amplitude (for a degree of hydration close to 1) is equal to A_{sd}. The values of A_{sd} shown in Table 5 indicate that BFS (C2) significantly increases the autogenous deformation. This is a well-known effect that has already been noted by other researchers [23, 16]. On the other hand, C3 is characterised by a lower shrinkage development. This is partially due to the dilution effect of LMF, since it only contains 70% of CEMI in comparison with C1. This low shrinkage can also be explained by the lower porosity of C3 in comparison with C1 due to the filler effect of LMF. Finally, this observation can also be attributed to the increased water available for cement hydration due to the inert nature of LMF, resulting in coarser porosity and higher saturation degree, and therefore lower capillary pressure. The combination of these three mechanisms results in a development of the autogenous shrinkage of C3 being less than half of C1. Finally, C4 has a lower slope than C2, due to the substitution of 30% of BFS by LMF between both compositions. However, as indicated by the heat release measurements, no dilution effect of LMF can be observed in C4 in comparison with C2. Therefore, the lower shrinkage development of C4 is attributed mainly to the filler effect of LMF, which is significantly finer than BFS.

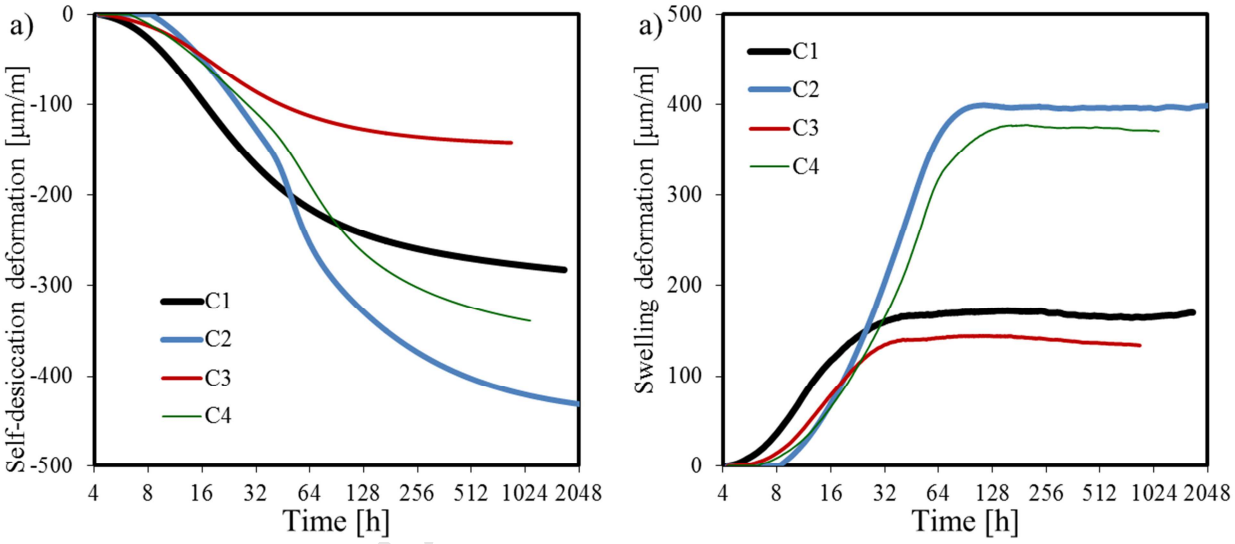

Figure 7. Contribution to the autogenous deformation of (a) self-desiccation and (b) swelling

3.3.2. *Swelling deformation*

Considering equations 5-8, the swelling deformation ε_{sw} can be computed by subtracting the thermal and self-desiccation deformation from the measured deformation. As a result, S-shaped curves appear in Figure 7b. The swelling deformation progressively increases until stabilizing at a fixed value after a few hours up to a few days, depending on the composition. These curves confirm that according to this methodology, contrary to the self-desiccation mechanism, the swelling only occurs during the first days of hydration, and do not contribute to the long term development of the autogenous deformation. Regarding the amplitude of this swelling A_{sw}, its value shown in Table 6 can be obtained mathematically as the y-axis intercept of the line fitting the linear ε_{au}-α curve.

Table 6. Amplitude of the swelling deformation

	C1	C2	C3	C4
A_{sw} [µm/m]	168±19	397±22	142±12	376±23

As stated previously, the error on the determination of the swelling amplitude A_{sw} is higher than in the case of the self-desiccation amplitude A_{sd}. However, clear trends appear when replacing CEMI by LMF or BFS. First, BFS induces a very significant increase of ε_{sw}. This has already been pointed out by other authors, and is generally attributed to the additional formation of ettringite in presence of slag [23]. Since the hydration of C2 is slower in comparison with C1, the swelling peak is delayed. On the other hand, LMF induces a slight decrease of the swelling amplitude. In the same way, when combining BFS and LMF in C4, ε_{sw} has an overall trend similar to its counterpart without LMF. This indicates that LMF has no significant effect on ε_{sw}. This observation is not only inconsistent with the swelling mechanism related to the filler adsoprtion of water [13], but also counter-intuitive considering the total autogenous deformation shown in Figure 5. In that figure, C3 shows a higher swelling peak than C1. This is explained by the very low self-desiccation deformation of C3. Indeed, when no LMF is present (C1), the swelling is mostly counter-balanced by large self-desiccation deformations at early-age. However, in C3, the swelling peak observed in the total autogenous deformation is most likely due to a decrease in the self-desiccation rather to an increase of ε_{sw}.

3.4.*Mechanisms of the swelling deformation*

The early age swelling deformation is generally attributed to at least one of the following mechanisms:

- measurement artefact,
- absorption of bleeding water [11],
- water adsorption by filler [12, 13],
- CH growth [14],
- primary ettringite formation [14, 15].

The measurements have been confronted in Figure 6b to another test setup, which has confirmed that the swelling is not due to an artefact. The second mechanism can be ruled out due to the fact that the limited w/c ratio used in this study induced no measurable bleeding water. As discussed previously; according to the third mechanism, the presence of limestone filler should increase the water adsorption around small particles, whereas LMF is observed to have only a limited (if not slightly decreasing effect) on the amplitude of the swelling deformation. Therefore, this mechanism is not predominant in this case. Furthermore, the CH growth is known to produce cement matrix expansions during hydration. However, compositions containing BFS generally show higher swelling deformations while exhibiting very low CH content due to its consumption by the hydration of the slag. This was observed by TGA on all tested compositions (Figure 8). Based on these results, the CH growth mechanism for the swelling deformation can be ruled out for three main reasons:

- the compositions with BFS show a decreasing CH content after 24h, while they still exhibit an increasing swelling at that point. Therefore, even if it still could reasonably be argued that CH induces swelling, this demonstrates that CH growth is not the only mechanism in play,
- the portlandite content is due to the Portland cement hydration, and it therefore occurs almost simultaneously in all compositions, proportionally to the amount of CEM I present in the mix(Figure 8). However, the swelling in presence of BFS occurs significantly later than without BFS. This contributes to the idea that CH growth is not the main mechanism of early age swelling,
- the compositions containing BFS exhibit the lowest CH content due to their very low CEM I content. However, these same compositions present by far the highest swelling

deformation. There is therefore no evidence of a relationship between the CH formation and the swelling behaviour observed in the tested concretes.

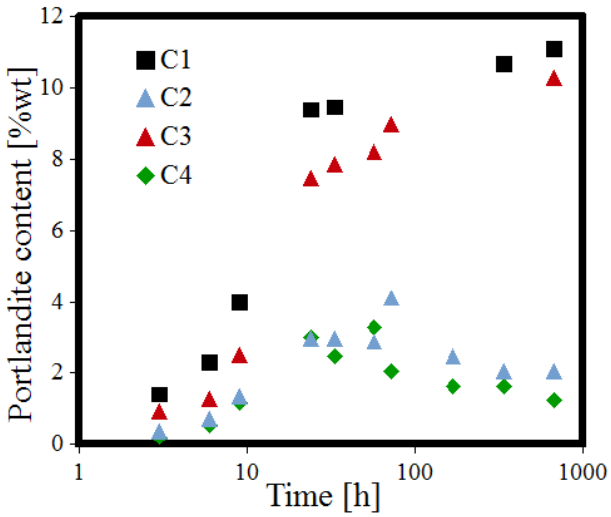

Figure 8. Portlandite content as a function of time for each composition

The primary ettringite formation is therefore the most plausible explanation for the observed swelling deformation. It is known since the early 60's that the formation of ettringite is accompanied with an expansion. Originally, two mechanisms were proposed for this early age expansion. According to the crystal growth theory, the swelling in presence of ettringite is due to its formation around anhydrous or hydrated grains. Due to the porous aspect of ettringite (related to its needle-like structure), its volume occupies more space than its original constituents, and therefore induces a matrix expansion as soon as it comes in contact with another ettringite layer [15]. According to the swelling theory, ettringite forms as colloidal particles in through-solution. These high specific surface particles result in water adsorption and therefore to an apparent cement expansion [14]. Although the crystal growth theory is often considered to be the dominant mechanism, a combination of both theories is the most probable cause of ettringite swelling. This swelling is observed to depend on the amount of ettringite, on its formation mode (through-solution colloidal suspensions or topochemical crystal growth), all of which depend on the source nature and amount of Al^{3+} and SO^{3-} ions [30, 31]. Also, the swelling kinetics is highly dependent on the strength and stiffness of the paste in the vicinity of ettringite crystals [32]. Based on these facts, various mechanisms can be at the origin of the swellings observed in Figure 7.

First, the presence of LMF does not affect directly the amount or nature of SO^{3-} nor Al^{3+} ions in solution, and therefore induces a slight decrease in the swelling deformation, probably by dilution effect (lower amount of reactive content in the cement paste). This effect might be partly counterbalanced by the lower early age stiffness of concrete with LMF than without [07].

Secondly, the presence of BFS in concrete affects the amount and nature of the ions in solution. The significantly higher amount of swelling in its presence might be the result of the production of a different nature or structure of ettringite, of the increased amount of ettringite produced, or finally of the lower stiffness of the matrix in presence of BFS [07]. One of the possible ways to understand more deeply the role of BFS on the swelling deformation would be to quantify the ettringite content in each composition. However, the possibilities of experimental quantification of the ettringite content are quite reduced. Indeed, on cement pastes, the selective dissolution,

thermogravimetric analysis or X-ray diffraction all show experimental artefacts allowing in the best case scenario semi-quantitative results [33].

By comparing the heat flow and the swelling deformation measurements, it can be observed that the main swelling peak (Figure 7b) occurs during the second shoulder in the heat flow curves (Figure 4). This shoulder corresponds to the hydration of the aluminates, which indicate the depletion of gypsum thus accelerating C3A hydration which was partially arrested by the adsorption of sulphate ions on the surface of the reactant particle [34]. When the adsorbing sulphate ions are released this accelerates the ettringite formation along with the formation of AFm [24]. This occurs between 10-15h for C1, 35-65h for C2, 15-30h for C3 and 40-80h for C4. Most of the swelling occurs at the time where ettringite is formed. Based on this observation, it can be supposed that ettringite is at the origin of this swelling. This does not exclude that other hydration products contribute to the swelling as well.

In order to have additional information, qualitative analysis is performed by TGA. The dehydration of ettringite occurs for a temperature close to 95°C. However, this temperature also corresponds to the dehydration of C-S-H and AFm [35, 36]. As shown in Figure 9, the amount of ettringite, C-S-H and AFm increases within the first hours after mixing, and up to a few days. Then, it stabilizes, so that no significant difference can be observed between up to 28d. An indicator of the ettringite content is chosen as the difference between the relative mass at 105°C (m_{105}) and the relative mass at 85°C (m_{85}). This indicator is computed for each measurement (between 3h and 28d) and compared to the autogenous swelling deformation in Figure 10.

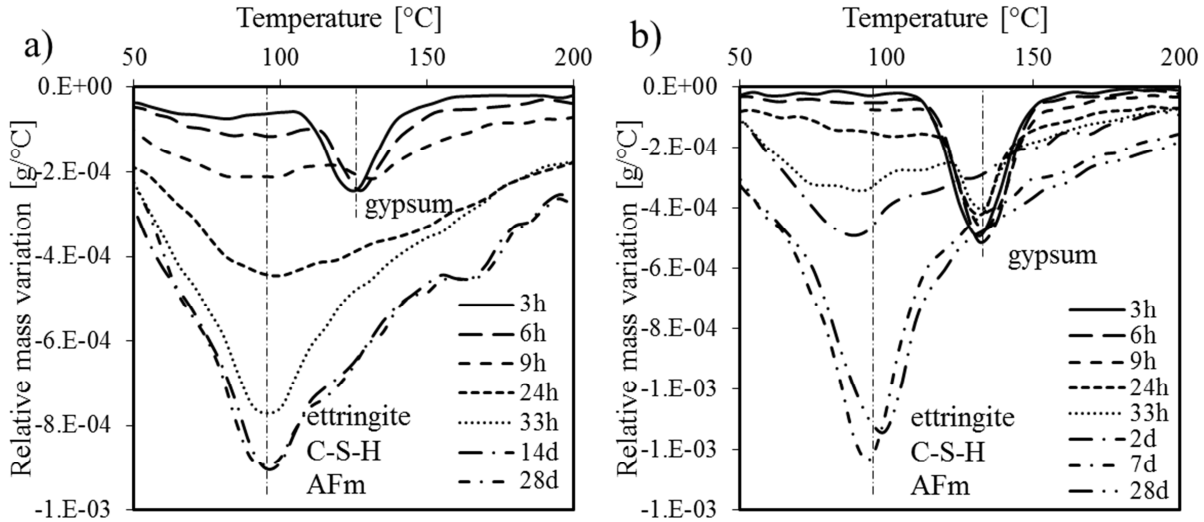

Figure 9. Relative mass variation related to the ettringite, C-S-H, AFm and gypsum from TGA for compositions a) C1 and b) C4

This confirms that the time frame during which the swelling occurs corresponds to the time when most of the ettringite is formed. This is only a qualitative correlation since the mass loss between 85°C and 105°C cannot be attributed only to the ettringite, but also to the C-S-H and AFm. This correspondence is verified for all compositions, with and without LMF or BFS. These evidences confirm that the ettringite formation is the main mechanism at the origin of the swelling. This is further validated by the decrease of gypsum, which is consumed by the formation of ettringite. The peak related to gypsum decreases between 3h and 24h for C1 and between 3h and 48h for C4. However, in the presence of slag, it can be observed that swelling continues shortly after depletion of the gypsum content. The absence of gypsum prevents additional ettringite

formation, and induces a transformation of AFt to AFm phases [24]. This indicates that this transformation might also contribute, to a lesser extent, to the swelling deformation.

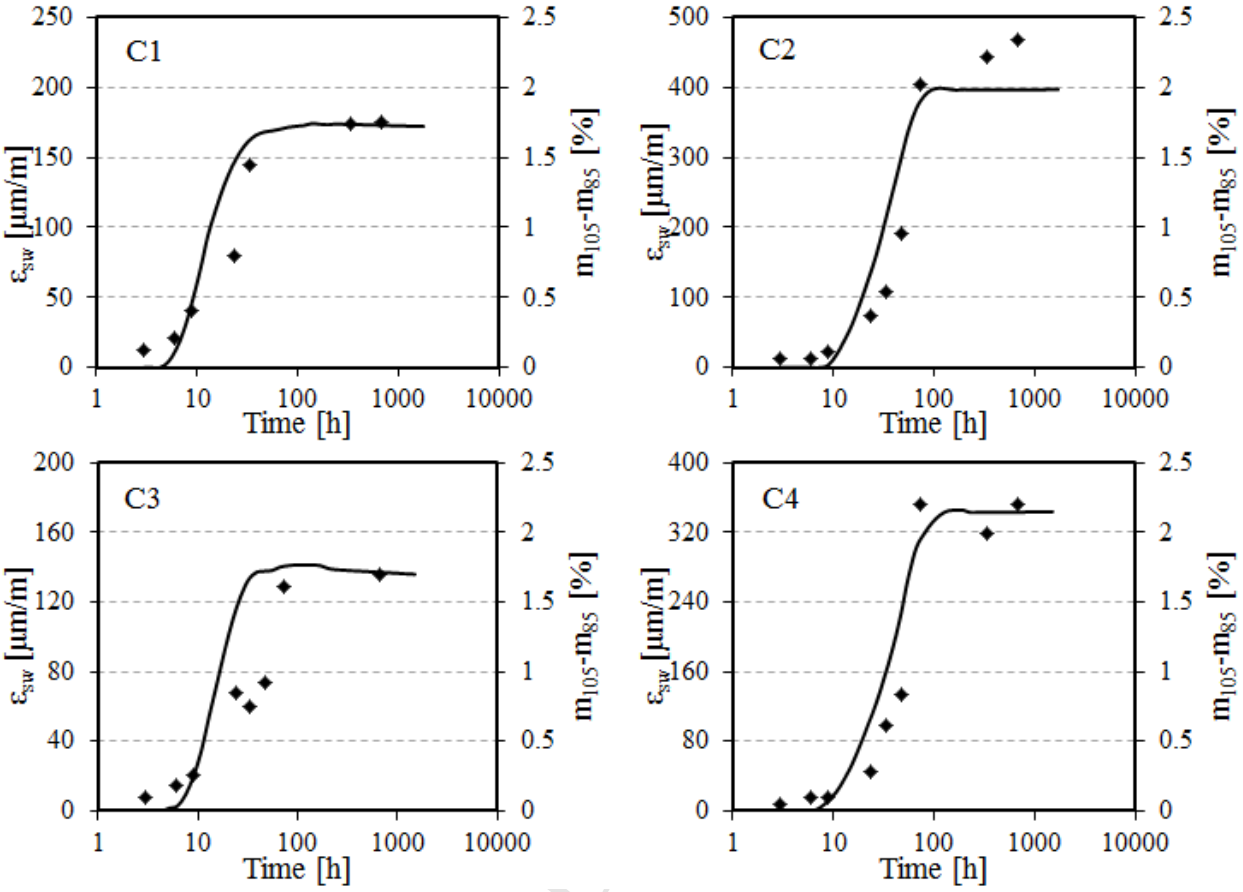

Figure 10. Comparison between ettringite-related mass loss from TGA (between 85°C and 105°C) and autogenous swelling deformation

Regarding the effect of SCM, it can be noticed that LMF does not generate swelling. Indeed, similar expansion is generated for an equivalent ettringite amount between C1 and C3, and between C2 and C4. However, BFS induces a significantly higher swelling generation for similar ettringite content. One possible explanation would be that in the presence of slag, ettringite is formed when the cement matrix has lower rigidity. This is consistent with the low early age E-modulus measured on the same mix compositions and presented elsewhere [07]. Therefore, a same amount of ettringite would result in higher swelling. Another possibility is that the actual nature and structure of ettringite is different with and without slag.

In order to understand this difference, SEM analyses are performed on C1 and C2 at 2 days of hydration. At that time, the swelling with slag (C2) is higher than the one of C1 (Figure 7b), but the degree of hydration of C2 is lower than C1 (Figure 4). The results of these experiments show that needle-like ettringite is present in both concrete in high quantity (Figure 12). However, when slag is introduced, a denser network of needles is noticeable. This network is composed of shorter needles than in absence of slag, probably due to the higher degree of hydration of C1 at that point. On the one hand, the denser ettringite network might be the cause of its higher swelling. On the other hand, if ettringite is the main cause of swelling, the larger needles in C1 should have induced higher swelling. The lack of a clear relationship between the presence of ettringite and the macroscopic swelling confirms that a preponderant property in its development is the stiffness of the surrounding matrix. If ettringite develops when the stiffness of concrete is

too high, it might not result in any swelling at all, whereas in the case of C2, the slow increase in stiffness allows ettringite to induce such swelling.

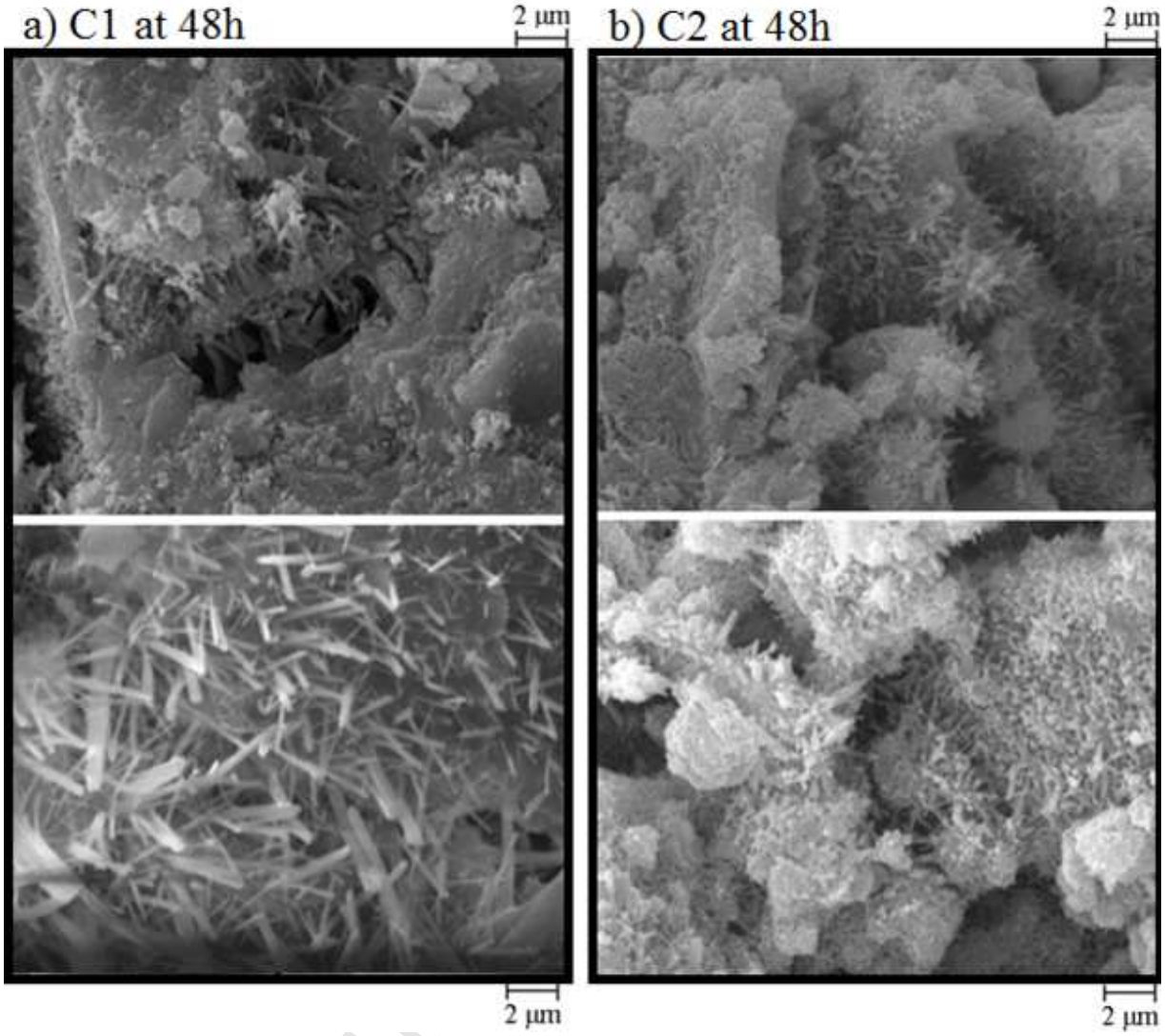

Figure 12. SEM observation of the ettringite at 48h on concrete a) without slag and b) with slag made at 4MAT lab, ULB.

3.5.*Modelling the autogenous deformations*

The modelling approach for the self-desiccation was previously described in equation 8, as it is part of the autogenous deformation decoupling strategy. Since it has been established that the swelling is mostly due to the ettringite formation which results from the cement hydration, it makes sense to study the evolution of ε_{sw} as a function of α. The relative swelling deformation ε_{sw}/A_{sw} displayed in Figure 13 is characterized by an s-shaped swelling as a function of the degree of hydration. The fast increase of the swelling is attributed to the initially large production of ettringite. For higher degree of hydration, the ettringite production rate decreases, and the overall stiffness of the cement matrix increases. At a degree of hydration between 0.6 and 0.7, the expansion reaches a plateau which is explained by a combination of these two mechanisms. It is observed that the relative swelling development is initially slowed down by the presence or LMF or BFS, and even slower in the presence of both.

It is chosen to model the swelling as a s-shaped function of the degree of hydration, consisting in a rapid increase of the production rate for low degree of hydration, and a tangent value of A_{sw}. The sigmoid or logistic functions as well as Gompertz curves are classical examples of such behaviour. However, these mathematical expressions are symmetrical and have no explicit conditions according to which the swelling at α_0 is equal to 0. The chosen expression for modelling the swelling is shown in equation 9.

$$\frac{\varepsilon_{sw}}{A_{sw}} = 1 - e^{-a\,.\tilde{\alpha}^b} \quad (9)$$

It is preferred to the others based on its ability to impose an initial value of 0, and to depend on two parameters *a* and *b*. The first parameter controls the degree of hydration at which the plateau occurs (for higher value of *a*, the plateau is reached sooner), while the second parameter controls the rate at which the swelling develops (for higher value of *b*, the swelling develops more slowly). The interest of this model is that based on Figure 13, it appears that parameter *a* is independent on the concrete composition, and can therefore be chosen as a constant. Only parameter *b* is function of the presence of SCM.

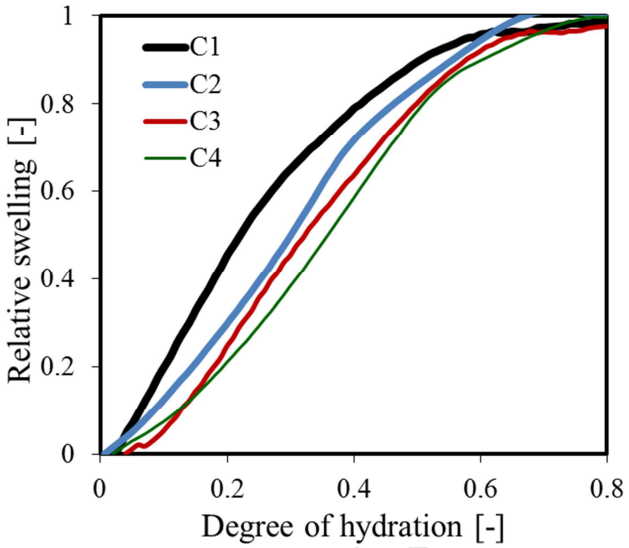

Figure 13. Evolution of the relative swelling deformation as a function of degree of hydration

The values of the parameters *a* and *b* are shown in Table 7. The parameter *a* is fixed at 7 for all compositions since it mathematically corresponds to a fast decrease of the swelling deformation rate around a degree of hydration of 0.6 (plateau of swelling). The values of parameter *b* increase with the presence of BFS, LMF, and even more when both are present. This is in agreement with the observation that the tested SCM delay the swelling development for a given degree of hydration. In order to improve the understanding of the relationship between mix composition (SCM amount and nature, w/c ratio) and the value of parameters *a* and *b*, further tests should be performed. At this stage, these two parameters are considered as fitting parameters without precise physical interpretation.

Table 7. Parameters of the relative swelling model

	C1	**C2**	**C3**	**C4**
b	1.45 ± .15	1.84 ± .12	1.81 ± .06	2.05 ± .05

a 7 7 7 7

$$\varepsilon_{au} = \underbrace{A_{sd}.\tilde{\alpha}}_{\varepsilon_{sd}} + \underbrace{A_{sw}.\left(1 - \mathrm{e}^{-7\,\tilde{\alpha}^{b}}\right)}_{\varepsilon_{sw}} + \varepsilon_{th} \qquad (10)$$

Ultimately, the new unified model for the autogenous deformations can be written in the form of equation 10, based on equations 6-9. It consists in a self-desiccation contribution, linearly dependent on the degree of hydration, and on a chemo-physical swelling deformation, related to the hydration degree until the swelling plateau is reached through an s-shaped curve. Based on experimental observations, the degree of hydration at which the swelling plateau occurs is close to 0.6. This means that according to the model, the ettringite formation generates expansion only if it is formed at a degree of hydration under this value.

The relevance of this model is confirmed in Figure 14, where the experimental curves for the swelling, self-desiccation and total deformations (continuous lines) are confronted to the corresponding modelled curves (dashed lines) for each compositions. The total apparent autogenous deformation results from two different mechanisms, which can be considered as independent and superimposable.

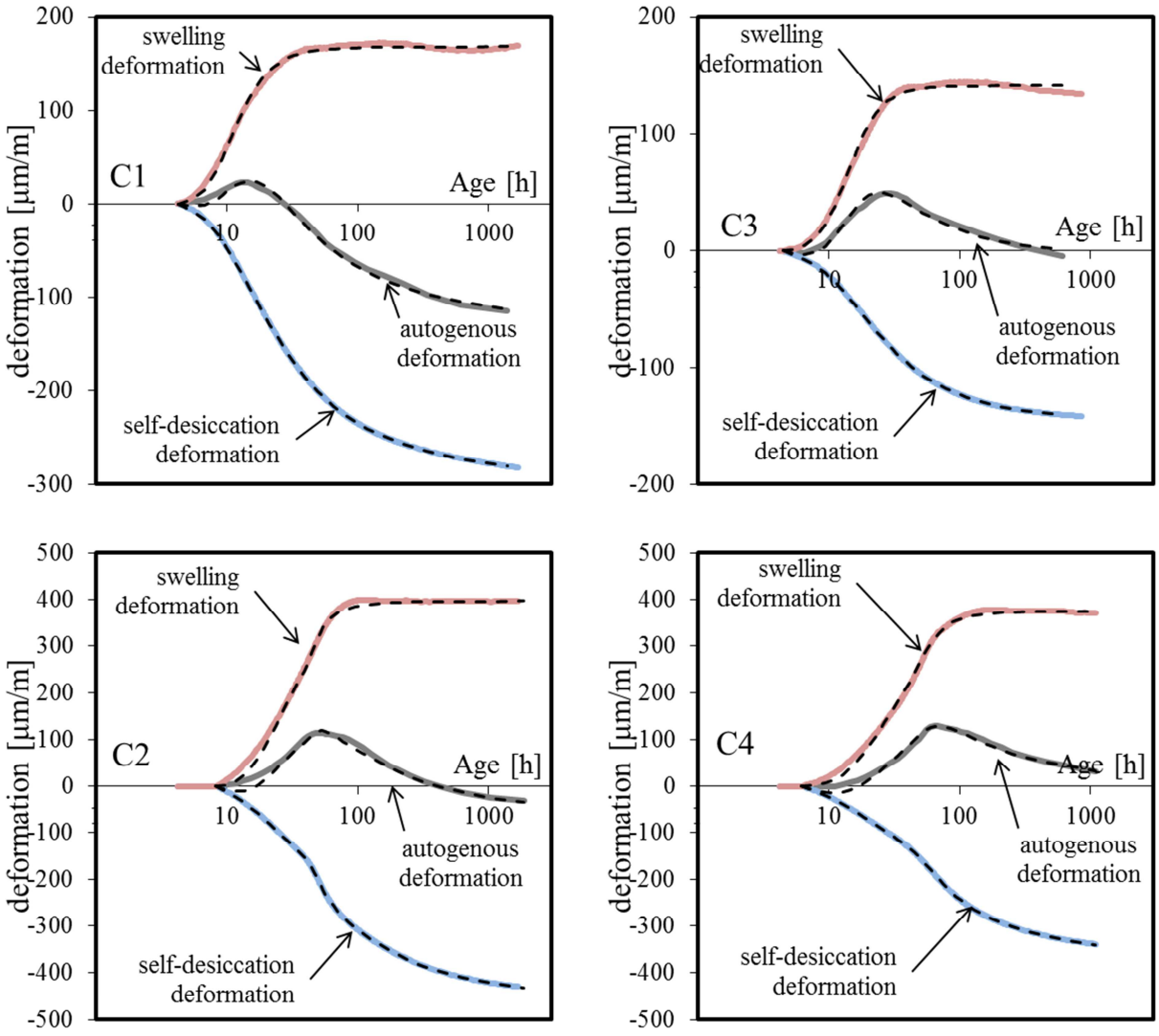

Figure 14. Comparison of the developed model with experimental results for the swelling deformation, self-desiccation deformation and total autogenous deformation (continuous lines for experimental values, dashed lines for modelled curves)

4. Conclusion

In this paper, a new methodology is developed to decouple the self-desiccation deformation from the swelling deformation in autogenous conditions. Both phenomena are closely related to the advancement of the hydration reactions, whether concrete contains only Portland cement, or a combination of Portland cement, limestone filler and/or blast-furnace slag. The main conclusions of this paper are that:

- The self-desiccation deformation occurs as a linear function of the advancement degree of hydration between at least 0.7 and 0.95, independently on the presence of mineral additions.
- The swelling deformation results from chemo-mechanical couplings of the ettringite formation, combining the growth of needle-like crystals generating internal pressure on the cement matrix, and the resistance of the matrix to this growth due to the concrete stiffness.
- The swelling is observed to occur from the setting time and up to a degree of hydration close to 0.6.
- Limestone filler tends to decrease moderately the swelling deformation and reduces consequently the self-desiccation deformation. The former is contrary to mechanism of swelling by water adsorption on the filler powder [13], which could not be confirmed in this study.
- Blast-furnace slag significantly increases both the swelling and self-desiccation behaviour. While these are common observations, this methodology allows quantifying these effects, indicating that the higher swelling in presence of BFS is not only due to the increased amount of ettringite, but also to the lower stiffness of the concrete at the time it is formed, therefore resulting in higher expansion.

In light of these observations, a unified hydration-based model is proposed for the modelling of the autogenous deformations of concrete with or without supplementary cementitious materials, from the very early age to several weeks. This new model relies on three main parameters: the amplitude of the self-desiccation deformation, the amplitude of the swelling deformation, and the kinetics of the swelling development.

Author Contributions

Jérôme Carette performed the BTJADE and isothermal calorimetry experiments at ULB, developed the data treatment methodology and the modelling strategy and wrote the paper under the supervision of Stéphanie Staquet.

Shiju Joseph performed the TGA experiments at KUL under the supervision of Özlem Cizer. They contributed to the analysis and discussions, in particular of section 3.4.

Acknowledgments

The authors would like to thank the Belgian Fund for Scientific Research (FNRS) and the Fund David & Alice Van Buuren for their financial support, as well as Marie-Paule Delplancke-Ogletree (4MAT, ULB) and Patrizio Madau (4MAT lab, ULB) for the SEM measurements.

590 **References**

591 [01] Menéndez, G.; Bonavetti, V. & Irassar, E., Strength development of ternary blended cement
592 with limestone filler and blast-furnace slag, Cement and Concrete Composites, 2003, 25, 61 – 67

593 [02] Carrasco, M.; Menéndez, G.; Bonavetti, V. & Irassar, E. Strength optimization of "tailor-
594 made cement" with limestone filler and blast furnace slag, Cement and Concrete Research, 2005,
595 35, 1324 – 1331

596 [03] Gao, Y.; Schutter, G. D.; Ye, G.; Yu, Z.; Tan, Z. & Wu, K. A microscopic study on ternary
597 blended cement based composites, Construction and Building Materials, 2013, 46, 28 – 38

598 [04] Courard, L. & Michel, F. Limestone fillers cement based composites: Effects of blast
599 furnace slags on fresh and hardened properties, Construction and Building Materials, 2014, 51,
600 439 – 445

601 [05] Carette J & Staquet S., Monitoring the setting process of eco-binders by ultrasonic P-wave
602 and S-wave transmission velocity measurement: Mortar vs concrete, Construction and Building
603 Materials, 2016, 110, 32-41

604 [06] Carette J. & Staquet S., Monitoring and modelling the early age and hardening behaviour of
605 eco-concrete through continuous non-destructive measurements: Part I. Hydration and apparent
606 activation energy, Cement and Concrete Composites, 73, pp. 10-18, 2016

607 [07] Carette J. & Staquet S., Monitoring and modelling the early age and hardening behaviour of
608 eco-concrete through continuous non-destructive measurements: Part II. Mechanical behaviour,
609 Cement and Concrete Composites, 73, pp. 1-9, 2016

610 [08] Mounanga, P.; Bouasker, M.; Pertue, A.; Perronnet, A. & Khelidj, A. Early-age autogenous
611 cracking of cementitious matrices: physico-chemical analysis and micro/macro investigations,
612 Materials and Structures, Springer Netherlands, 2011, 44, 749-772

613 [09] Bouasker, M.; Khalifa, N. E. H.; Mounanga, P. & Kahla, N. B. Early-age deformation and
614 autogenous cracking risk of slag-limestone filler-cement blended binders, Construction and
615 Building Materials, 2014, 55, 158 – 167

616 [10] Laurent Barcelo, Micheline Moranville, Bernard Clavaud, Autogenous shrinkage of
617 concrete: a balance between autogenous swelling and self-desiccation, Cement and Concrete
618 Research, 2005, 35, 177–183

619 [11] Bjøntegaard, Ø., Hammer, T. & Sellevold, E. J., 2004. On the measurement of free
620 deformation of early age cement paste and concrete. Cement and Concrete Composites, 26, 427-
621 435.

622 [12] Esping, O., 2008. Effect of limestone filler BET (H2O)-area on the fresh and hardened
623 properties of self-compacting concrete. Cement and Concrete Research, 38, 938-944.

624 [13] Craeye, B. et al., 2010. Effect of mineral filler type on autogenous shrinkage of self-
625 compacting concrete. Cement and Concrete Research, 40, 908-913.

626 [14] Mehta, P., 1973. Mechanism of expansion associated with ettringite formation. Cement and
627 Concrete Research, 3, 1-6.

628 [15] Bentur, A. & Ish-Shalom, M., 1974. Properties of type K expensive cement of pure
629 components II. Proposed mechanism of ettringite formation and expansion in unrestrained paste
630 of pure expansive component. Cement and Concrete Research, 4, 709-721.

631 [16] Y.; Hansen, W.; Biernacki, J. J. & Schlangen, E. Unified Shrinkage Model for Concrete
632 from Autogenous Shrinkage Test on Paste with and without Ground-Granulated Blast-Furnace
633 Slag ACI Materials Journal, 2011, 108, 13-20

[17] fib Bulletin 65, 2010. Model code 2010 – final draft, vol. 1; 2012. 350 pages, ISBN: 978-2-88394-105-2

[18] Chu, I., Kwon, S. H., Amin, M. N. & Kim, J.-K., 2012. Estimation of temperature effects on autogenous shrinkage of concrete by a new prediction model. Construction and Building Materials , 35(0), pp. 171-182.

[19] Z.Liu, W. Hansen, Aggregate and slag cement effects on autogenous shrinkage in cementitious materials, Construction and Building Materials, 121, pp. 429–436, 2016

[20] Lura, P., Jensen, O. M. & Breugel, K. v., 2003. Autogenous shrinkage in high-performance cement paste: An evaluation of basic mechanisms. Cement and Concrete Research , 33(2), pp. 223-232.

[21] Boulay, C., 2012. Test rig for early age measurements of the autogenous shrinkage of a concrete, Crack Control of Mass Concrete and Related Issues concerning Early-Age of Concrete Structures, RILEM Publications, 111-122.

[22] Baroghel-Bouny, V. et al., 2006. Autogenous deformations of cement pastes: Part II. W/C effects, micromacro correlations, and threshold values. Cement and Concrete Research, 36, pp. 123-136.

[23] Darquennes, A., Staquet, S., Delplancke-Ogletree, M.-P. & Espion, B., 2011. Effect of autogenous deformation on the cracking risk of slag cement concretes. Cement and Concrete Composites, 33, 368-379.

[24] A. Quennoz, , K. L. Scrivener, Interactions between alite and C3A-gypsum hydrations in model cements, Cement and Concrete Research, 44, pp. 46–54, 2013

[25] Staquet S, Delsaute B, Darquennes A, Espion B, Design of a revisited TSTM system for testing concrete since setting time under free and restraint conditions. In: Toutlemonde F, Torrenti J-M (eds) Proceedings of the RILEM-JCJ International Workshop ConCrack 3, pp 99–110, 2012

[26] Loukili, A.; Khelidj, A. & Richard, P. Hydration kinetics, change of relative humidity,and autogenous shrinkage of ultra-high-strength concrete Cement and Concrete Research , 1999, 29, 577 – 584

[27] Kong, Xm., Zhang, Zl. & Lu, Zc., Effect of pre-soaked superabsorbent polymer on shrinkage of high-strength concrete, Materials and Structures, 48, pp 2741–2758, 2015

[28] E.A.B. Koenders, Simulation of volume changes in hardening cement-based

materials (Ph.D. thesis), Delft University of Technology, Delft, The Netherlands,

1997.

[29] P. Lura, Autogenous deformation and internal curing of concrete (Ph.D. thesis),

Delft University of Technology, Delft, The Netherlands, 2003.

[30] Odler, I. & Colán-Subauste, J., Investigations on cement expansion associated with ettringite formation. Cement and Concrete Research, 29(5), pp. 731-735, 1999.

[31] Evju, C. & Hansen, S., The kinetics of ettringite formation and dilatation in a blended cement with Î²-hemihydrate and anhydrite as calcium sulfate. Cement and Concrete Research , 35(12), pp. 2310-2321, 2005.

[32] Min, D. & Mingshu, T., Formation and expansion of ettringite crystals. Cement and Concrete Research, 24(1), pp. 119-126. 1994.

676 [33] Odler, I. & Abdul-Maula, S., Possibilities of quantitative determination of the AFt-
677 (ettringite) and AFm-(monosulphate) phases in hydrated cement pastes. Cement and Concrete
678 Research, 14(1), pp. 133-141. 1984.

679 [34] H. Minard, S. Garrault, L. Regnaud, A. Nonat, Mechanisms and parameters controlling the
680 tricalcium aluminate reactivity in the presence of gypsum, Cement and Concrete Research, 37,
681 pp1418–1426, 2007.

682 [35] B. Lothenbach, G. Le Saout, E. Gallucci, K. Scrivener, Influence of limestone on the
683 hydration of Portland cements, Cement and Concrete Research, 38, pp. 848-860, 2008

684 [36] A Practical Guide to Microstructural Analysis of Cementitious Materials, edited by K.
685 Scrivener, R. Snellings, B. Lothenbach, CRC Press, 2015